

See discussions, stats, and author profiles for this publication at: <https://www.researchgate.net/publication/236123875>

# Alucone Alloys with Tunable Properties Using Alucone Molecular Layer Deposition and Al<sub>2</sub>O<sub>3</sub>Atomic Layer Deposition

ARTICLE in THE JOURNAL OF PHYSICAL CHEMISTRY C · FEBRUARY 2012

Impact Factor: 4.77 · DOI: 10.1021/jp209003h

---

CITATIONS

36

READS

166

---

## 4 AUTHORS, INCLUDING:



[Byunghoon Yoon](#)

University of Colorado Boulder

33 PUBLICATIONS 1,016 CITATIONS

[SEE PROFILE](#)



[Virginia R. Anderson](#)

United States Naval Research Laboratory

7 PUBLICATIONS 90 CITATIONS

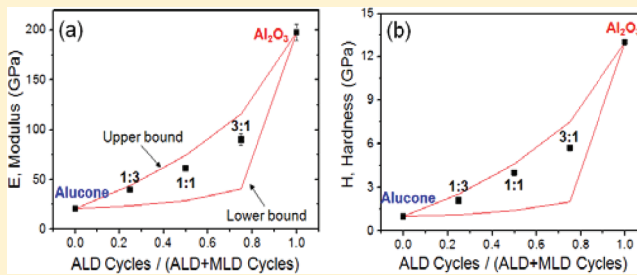
[SEE PROFILE](#)

# Alucone Alloys with Tunable Properties Using Alucone Molecular Layer Deposition and $\text{Al}_2\text{O}_3$ Atomic Layer Deposition

Byoung H. Lee,<sup>†</sup> Byunghoon Yoon,<sup>†</sup> Virginia R. Anderson,<sup>†</sup> and Steven M. George\*,<sup>†,‡</sup>

<sup>†</sup>Department of Chemistry and Biochemistry and <sup>‡</sup>Department of Chemical and Biological Engineering, University of Colorado, Boulder, Colorado 80309-0215, United States

**ABSTRACT:** Ultrathin and conformal hybrid organic–inorganic thin films can be deposited by molecular layer deposition (MLD) techniques. By combining the hybrid organic–inorganic MLD process with an inorganic atomic layer deposition (ALD) process, ALD/MLD alloy films can be deposited that have an adjustable organic–inorganic composition. These alloys have tunable properties that may be useful for designing various functional films. In this study, alucone MLD using trimethylaluminum (TMA) and ethylene glycol (EG) was employed together with  $\text{Al}_2\text{O}_3$  ALD using TMA and  $\text{H}_2\text{O}$  to deposit alucone alloys at 135 °C. The surface species and film growth were examined using *in situ* Fourier transform infrared spectroscopy. The mass gain for each reactant exposure during film growth was also monitored using *in situ* quartz crystal microbalance (QCM) in a viscous flow reactor. The composition of the alucone alloy was varied by adjusting the relative number of ALD and MLD cycles in the reaction sequence. Alucone alloys were grown using relative numbers of ALD and MLD cycles varying from 1:3 to 6:1 (TMA/ $\text{H}_2\text{O}$ :TMA/EG). These alucone alloys displayed varying density, refractive index, elastic modulus, and hardness. The density and refractive index changed from 1.6 g/cm<sup>3</sup> and  $n = 1.45$  for pure alucone to 3.0 g/cm<sup>3</sup> and  $n = 1.64$  for pure  $\text{Al}_2\text{O}_3$ , respectively. The elastic modulus and hardness varied from  $21 \pm 8$  GPa and  $1.0 \pm 0.1$  GPa for pure alucone to  $198 \pm 8$  GPa and  $13.0 \pm 0.2$  GPa for pure  $\text{Al}_2\text{O}_3$ , respectively. These results demonstrate the potential of ALD/MLD alloy films to provide tunable properties for many functional film applications.



## I. INTRODUCTION

Atomic level controlled and conformal inorganic films can be grown using atomic layer deposition (ALD) techniques.<sup>1–5</sup> A wide variety of inorganic materials including oxides, nitrides, and metals can be deposited using ALD for many thin film applications.<sup>6</sup> Ultrathin organic films with excellent conformality can also be grown using molecular layer deposition (MLD) techniques.<sup>7</sup> MLD growth was originally developed for a variety of all-organic polymers including polyamides<sup>8,9</sup> and polyimides<sup>10,11</sup> using bifunctional organic monomers. The principles of ALD and MLD are similar. Both ALD and MLD depend on sequential, self-limiting surface reactions.<sup>7</sup> These film growth methods allow the film thickness to be controlled at the atom or molecular fragment level. The self-limiting nature of the surface reactions is also responsible for the conformality of the deposition.

The organic precursors used in MLD can also be combined with inorganic ALD precursors to prepare hybrid organic–inorganic films.<sup>7,12–19</sup> For example, a large family of materials can be prepared using organic alcohol precursors together with organometallic precursors to deposit metal alkoxide polymeric films. These metal alkoxides are known as “metalcones”.<sup>20</sup> The “alucones” and “zincones” are two of examples of this metalcone family.<sup>12,18,21</sup> Carboxylic acids can also serve as the organic precursor together with various organometallic precursors to define another class of hybrid organic–inorganic films.<sup>13,14</sup> The growth of these hybrid organic–inorganic films

is considered an MLD process since this growth incorporates a molecular fragment during the self-limiting sequential reactions.

Hybrid organic–inorganic films can also be deposited by combining ALD and MLD processes. This combination is performed by interspersing the ALD cycles and MLD cycles. Depending on the frequency of transition between ALD and MLD cycles, the hybrid organic–inorganic films can either be homogeneous alloys or multilayered laminates. The fraction of the organic and inorganic constituents can be tuned by varying the relative number of ALD and MLD cycles. The ability to mix and match ALD and MLD processes offers a wide variety of possibilities for tuning film composition, film structure, and film properties. This ability to engineer films at the atomic level will be important for many thin film applications.

In this study, the growth and properties of alucone alloys were explored by combining  $\text{Al}_2\text{O}_3$  ALD and alucone MLD processes.  $\text{Al}_2\text{O}_3$  ALD was performed using trimethylaluminum (TMA) and  $\text{H}_2\text{O}$ .<sup>22–24</sup> Alucone MLD was accomplished using TMA and ethylene glycol (EG).<sup>12</sup> The composition of the alucone alloy was defined by the relative ratio of the TMA/ $\text{H}_2\text{O}$  ALD cycles and the TMA/EG MLD cycles. *In situ* quartz crystal microbalance (QCM) measurements and *in situ* Fourier transform infrared (FTIR) spectroscopy were used to

**Received:** September 17, 2011

**Revised:** December 24, 2011

**Published:** January 9, 2012



investigate the growth of the alucone alloys. X-ray reflectivity (XRR) was employed to determine the thickness and stability of the alucone alloy films. Transmission electron microscopy (TEM) was also used to examine the structure and conformality of the alloy films.

The properties of the alucone alloys were examined as a function of fraction of organic and inorganic composition. The density was measured using XRR, and the refractive index was monitored using spectroscopic ellipsometry. The elastic modulus and hardness were determined using nanoindentation studies. The properties were observed to vary between the pure  $\text{Al}_2\text{O}_3$  ALD film and the pure alucone MLD film. These results illustrate that thin film properties can be tuned over a wide range of values by combining inorganic ALD and organic MLD to fabricate hybrid organic–inorganic alloys.

## II. EXPERIMENTAL SECTION

### 1. Chemicals, Reactor, and Reaction Conditions.

Alucone alloys were fabricated using trimethylaluminum ( $\text{Al}(\text{CH}_3)_3$ ; 97%, Sigma-Aldrich), ethylene glycol ( $\text{HO}-(\text{CH}_2)_2\text{OH}$ ; Reagent Plus >99%, Sigma-Aldrich), and water ( $\text{H}_2\text{O}$ , Fisher Scientific HPLC grade). Ultrahigh purity  $\text{N}_2$  (Airgas) was used as the carrier gas in the viscous flow reactor and as the purge between reactant exposures. For *ex situ* analysis, the films were grown on boron-doped p-type Si(100) substrates with a thin native oxide (Silicon Valley Microelectronics, Inc.). The sample substrates were cleaved from intact Si wafers into 1 in.  $\times$  1 in. squares. Degreasing was performed using a 15 min dip in piranha solution (70% sulfuric acid and 30% hydrogen peroxide). The substrates were then rinsed with distilled  $\text{H}_2\text{O}$  and dried under nitrogen gas.

The alucone alloy films were deposited at 135 °C in a viscous flow ALD reactor that has been described in detail elsewhere.<sup>25</sup> The alucone alloy films were deposited using alternating TMA/ $\text{H}_2\text{O}$  exposures for  $\text{Al}_2\text{O}_3$  ALD and alternating TMA/EG exposures for alucone MLD. The exposure sequences are designated as  $(t_1, t_2, t_3, t_4)$  where  $t_1$  is the TMA exposure time,  $t_2$  is the purge time after the TMA exposure,  $t_3$  is the  $\text{H}_2\text{O}$  or EG exposure time, and  $t_4$  is the purge time after the  $\text{H}_2\text{O}$  or EG exposure. All times are in seconds. The reactant exposures for the quartz crystal microbalance (QCM) measurements were 1 s. A 40 s purge time was used after the reactant exposures. The reactant exposure times produced ~70–100 mTorr pressure transients above the base pressure of ~760 mTorr in the reactor under  $\text{N}_2$  flow. The QCM measurements determined that these dose times were sufficient to saturate the surface at the growth temperature of 135 °C.

The alucone alloys were defined by the ratio of ALD:MLD cycles. For example, the 1:1 alucone alloy was grown using an alternation of 1 cycle of  $\text{Al}_2\text{O}_3$  ALD and 1 cycle of alucone MLD. The reactant sequence of TMA/ $\text{H}_2\text{O}$ /TMA/EG for the 1:1 alucone alloy is shown in Figure 1. In comparison, the 2:1 alucone alloy was grown using an alternation of 2 cycles of  $\text{Al}_2\text{O}_3$  ALD and 1 cycle of alucone MLD. The reactant sequence for the formation of the 2:1 alucone alloy is TMA/ $\text{H}_2\text{O}$ /TMA/ $\text{H}_2\text{O}$ /TMA/EG.

**2. In Situ Thin Film Growth Analysis.** *In situ* FTIR studies were performed with a Nicolet Nexus 870 FTIR spectrometer equipped with a liquid- $\text{N}_2$ -cooled mercury–cadmium–telluride (MCT-B) infrared detector. Spectra were collected with a mirror speed of 1.8 cm/s and averaged over 100 scans using 4  $\text{cm}^{-1}$  resolution. The IR transparent windows on the viscous flow MLD reactor were KBr disks supplied by International

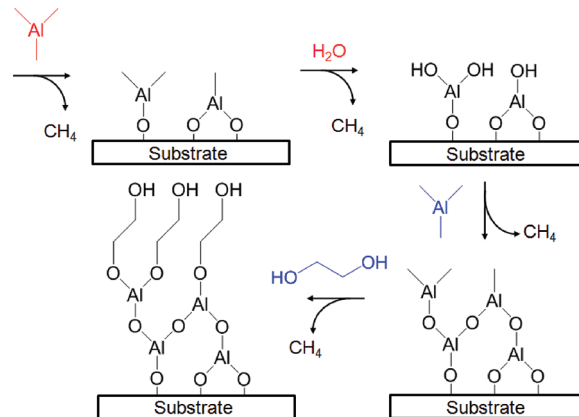


**Figure 1.** Schematic depicting 1:1 alucone alloy film growth using  $\text{Al}_2\text{O}_3$  ALD with TMA/ $\text{H}_2\text{O}$  and alucone MLD with TMA/EG.

Crystal Laboratories. The spectrometer setup was purged with dry and  $\text{CO}_2$ -free air delivered from a purge gas generator.

The transmission FTIR spectroscopy measurements required high surface area samples to obtain a sufficient signal-to-noise to monitor the surface species. The high surface area samples were approximately spherical  $\text{ZrO}_2$  nanoparticles with an average diameter of 25 nm. The nanoparticles were pressed into a stainless steel grid using methods described earlier.<sup>26</sup> The stainless steel grids supporting the  $\text{ZrO}_2$  nanoparticles were obtained from Tech Etch. The  $\text{ZrO}_2$  nanoparticles were obtained from Sigma-Aldrich.

The *in situ* QCM measurements were performed in the viscous flow reactor using a Maxtek TM400 thin film deposition monitor. The QCM sensors were quartz crystals with a polished Au face and a 6 MHz oscillation frequency (Colorado Crystal Corp.). The crystals were sealed into a Maxtek BSH-150 bakeable crystal housing and purged during deposition to avoid growth on the back side. During growth, the QCM was positioned horizontally and facing downward in the middle of the reactor.

**3. Ex Situ Film Analysis.** The thickness of alucone alloy films was determined by X-ray reflectivity (XRR) analysis. The XRR analysis was performed on films on Si(100) wafers using a Bede D1 high-resolution X-ray diffractometer from Bede Scientific, Inc. This X-ray diffractometer was equipped with a Cu X-ray tube and monochromator for  $\text{Cu K}\alpha$  radiation at  $\lambda = 1.54 \text{ \AA}$ . The XRR analysis was performed with  $\text{Cu K}\alpha_1$  radiation at  $\lambda = 1.540 \text{ \AA}$  after removing the  $\text{Cu K}\alpha_2$  radiation at  $\lambda = 1.544 \text{ \AA}$  using a channel cut crystal. A filament current of 40 mA and a voltage of 40 kV were used for the measurements. The XRR data were fit using the REFS fitting software from Bede Scientific, Inc., to extract the thickness, density, and roughness of the alucone alloy samples.

The refractive index,  $n$ , of alucone alloy films was obtained from *ex situ* reflective spectroscopic ellipsometry investigations. These measurements were performed using a J.A. Woollam M-2000 spectroscopic ellipsometer employing a spectral range from 240 to 1700 nm with an incidence angle of 75°. The refractive index values were derived from ellipsometric parameters for alucone alloy films deposited on silicon substrates using a Cauchy model.

Indentation of alucone alloy films was performed at room temperature using a nanoindenter (Nano Dynamic Contact Module (DCM), Agilent Technologies, Inc.) equipped with a diamond Berkovich tip.<sup>27</sup> These indentation measurements

characterized the elastic modulus and the hardness of the alloy films. Material properties were evaluated according to the Oliver–Pharr method. The Oliver–Pharr method used in conjunction with the continuous stiffness method (CSM) can characterize specimens over a range of thicknesses.<sup>28,29</sup> The nanoindentation technique is accurate to within about 5–10% of the actual values. Accuracy improves with the averaging of multiple indentations.

Alucone alloy films with thicknesses of ~250 nm were deposited onto Si(100) wafers at 135 °C. Immediately prior to indentation, the tip area function of the nanoindenter was calibrated using fused silica. Indents were performed up to a depth of 100 nm at the constant loading rate of 0.05 s<sup>-1</sup>. The maximum load was held for 10 s for stabilization and then rapidly unloaded at the rate of 250 μN s<sup>-1</sup>. The load was also held at 1% of the maximum load for 30 s to obtain a thermal drift correction. For all indentation experiments, test locations were separated by 100 μm to ensure isolation between the 10 test sites.

Because of surface roughness effects<sup>30</sup> and difficulties calibrating the tip area function,<sup>31</sup> artifacts are often observed in nanoindentation measurements of the hardness and elastic modulus for small indentation depths of <10–15 nm.<sup>32</sup> To avoid these artifacts, the property values were averaged at depths between 25 and 35 nm into the film. The property values were constant at penetration depths >15 nm into the film. This constancy argues that substrate effects are minimal.<sup>33</sup>

Transmission electron microscope (TEM) images of 1:1 alucone alloys were obtained by Prof. Myung M. Sung at Hanyang University. The samples for cross-sectional TEM studies were prepared by mechanical grinding and polishing. Ar-ion milling was then performed using a Gatan precision ion polishing system (PIPSSTM, model 691). The TEM image was acquired with a JEOL-2100F transmission electron microscope.

### III. RESULTS AND DISCUSSION

**1. Surface Chemistry.** The alucone alloy growth using Al<sub>2</sub>O<sub>3</sub> ALD and alucone MLD was studied using *in situ* transmission FTIR at a growth temperature of 135 °C on the high surface area ZrO<sub>2</sub> nanoparticles. The *in situ* FTIR spectra were recorded after each reactant exposure. Figure 2 shows the surface species during the 1:1 alucone alloy growth. The absolute FTIR spectra in Figure 2 are displayed for the initial hydroxylated ZrO<sub>2</sub> nanoparticle substrate and then after all the TMA, H<sub>2</sub>O, and EG exposures during the first two reaction sequences. These FTIR spectra are all referenced to the KBr windows and have been displaced for clarity in presentation.

Figure 2a shows the FTIR spectra of the hydroxylated ZrO<sub>2</sub> nanoparticles with a broad absorbance from O–H stretching vibrations at 3470–3810 cm<sup>-1</sup>. The O–H stretching vibrations are known to have a wide absorbance range on metal oxide surfaces.<sup>34–36</sup> After TMA exposure on the hydroxylated surface of the ZrO<sub>2</sub> nanoparticles, the absorbances from C–H stretching vibrations at 2800–3000 cm<sup>-1</sup> and from the methyl deformation of AlCH<sub>3</sub>\* at 1205 cm<sup>-1</sup> are present in Figure 2b.<sup>26</sup> Figure 2c shows that the H<sub>2</sub>O exposure reduces the C–H stretching vibration at 2800–3000 cm<sup>-1</sup> and the methyl deformation of AlCH<sub>3</sub>\* at 1205 cm<sup>-1</sup>. The H<sub>2</sub>O exposure also produces the O–H stretching vibration at 3200–3800 cm<sup>-1</sup>.<sup>26</sup> The subsequent TMA exposure produces spectral features in Figure 2d that are very similar to the spectral features observed after the first TMA exposure displayed in Figure 2b.

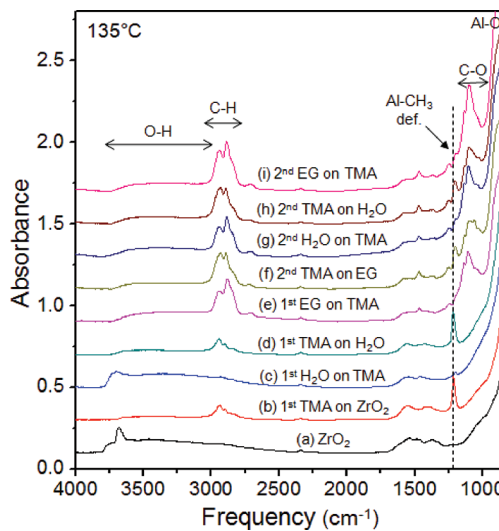


**Figure 2.** *In situ* absolute FTIR spectra during the growth of the 1:1 alucone alloy at 135 °C. Spectra of (a) initial ZrO<sub>2</sub> nanoparticles and (b) after initial TMA exposure on ZrO<sub>2</sub> nanoparticles. Spectra after subsequent (c) H<sub>2</sub>O exposure, (d) TMA exposure, and (e) EG exposure during the first sequence. Spectra after the subsequent (f) TMA exposure, (g) H<sub>2</sub>O exposure, and (h) TMA exposure, and (i) EG exposure during the second sequence.

After the first EG exposure, large absorbances are observed in Figure 2e at 2942 and 2879 cm<sup>-1</sup>, corresponding to the CH<sub>2</sub> asymmetric and symmetric stretching vibrations of the ethylene linkages between oxygen atoms in the aluminum alkoxide polymer.<sup>12</sup> In addition, the absorbance from the Al–O and C–O stretching vibrations are observed at 905 and 1100 cm<sup>-1</sup>, respectively. All the main vibrational features are assigned to –CH<sub>2</sub>–, C–O, or Al–O vibrational modes and consistent with the growth of an alucone alloy.<sup>12</sup> The spectra after the second sequence of TMA, H<sub>2</sub>O, TMA, and EG exposures are shown in Figure 2f–i, respectively. The absorbance from the methyl deformation of AlCH<sub>3</sub>\* is broadened considerably. The absorbance from the C–O stretching vibration also grows progressively.

The integrated absorbances of the methyl deformation of AlCH<sub>3</sub>\* species at 1250–1170 cm<sup>-1</sup> and the O–H stretching vibrations of AlOH\* and EG at 3800–3100 cm<sup>-1</sup> can be employed to monitor the surface reactions as a function of reactant exposure. The results shown in Figure 3 were obtained after preparing an Al<sub>2</sub>O<sub>3</sub> ALD surface on the ZrO<sub>2</sub> particles and then performing one complete TMA/H<sub>2</sub>O/TMA/EG sequence at 135 °C. Figures 3a,c show the integrated absorbance for the methyl deformation mode of AlCH<sub>3</sub>\* species versus the first TMA and second TMA exposure during the next TMA/H<sub>2</sub>O/TMA/EG sequence at 135 °C. The TMA exposures are defined by the number of TMA microdoses. Each TMA microdose was a 0.5 s exposure at 80 mTorr of partial pressure. Figures 3a,c demonstrate that both TMA reactions are self-limiting and reach completion after 8 microdoses for the first TMA exposure and 5 microdoses for the second TMA exposure.

The integrated absorbances from the O–H stretching vibrations versus H<sub>2</sub>O and EG exposures at 135 °C are shown in Figures 3b,d. The H<sub>2</sub>O and EG exposures are again defined by the number of H<sub>2</sub>O and EG microdoses. The H<sub>2</sub>O and EG partial pressures were 50 and 40 mTorr with 0.5 s microdoses, respectively. Figures 3b,d indicate that the H<sub>2</sub>O

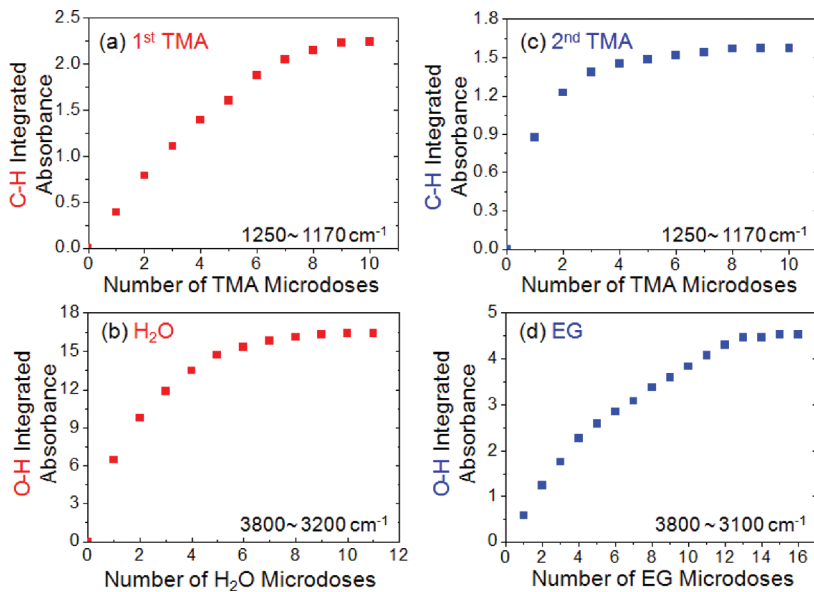


**Figure 3.** Self-limiting nature of surface reactions illustrated by integrated absorbances for (a) CH<sub>3</sub> deformation of AlCH<sub>3</sub>\* species versus first TMA exposure, (b) O–H stretching vibrations versus H<sub>2</sub>O exposure, (c) CH<sub>3</sub> deformation of AlCH<sub>3</sub>\* species versus second TMA exposure, and (d) O–H stretching vibrations versus H<sub>2</sub>O exposure. All exposures were performed during the growth of 1:1 alucone alloy film at 135 °C.

and EG reactions are self-limiting and reach completion after 8 H<sub>2</sub>O microdoses and 13 EG microdoses.

**2. Film Growth.** Figure 4 displays the mass gains during the deposition of the (a) 1:1 and (b) 3:1 alucone alloys during

show consistent mass gains after the TMA exposures. The mass gains after the H<sub>2</sub>O exposures were negligible. In contrast, the mass gains after the EG exposures are comparable to the mass gains after the TMA exposures.

The mass gains corresponding to the TMA, H<sub>2</sub>O, TMA, and EG exposures are in good agreement with the expected surface chemistry. For the growth of the 1:1 alucone alloy, mass gains of +12, -1, +10, and +10 ng/cm<sup>2</sup> are observed during the TMA, H<sub>2</sub>O, TMA, and EG exposures, respectively. Normalized using the total mass gain per cycle (MGPC), the mass ratios are  $\Delta m_{\text{TMA}}/\text{MGPC} = +0.387$ ,  $\Delta m_{\text{H}_2\text{O}}/\text{MGPC} = -0.032$ ,  $\Delta m_{\text{TMA}}/\text{MGPC} = +0.323$ , and  $\Delta m_{\text{EG}}/\text{MGPC} = +0.323$ . In comparison, the mass ratios predicted by the surface chemistry illustrated in Figure 1 are  $\Delta m_{\text{TMA}}/\text{MGPC} = +0.285$ ,  $\Delta m_{\text{H}_2\text{O}}/\text{MGPC} = +0.018$ ,  $\Delta m_{\text{TMA}}/\text{MGPC} = +0.285$ , and  $\Delta m_{\text{EG}}/\text{MGPC} = +0.411$ . The measured  $\Delta m_{\text{TMA}}/\text{MGPC}$  value is slightly higher, the measured  $\Delta m_{\text{H}_2\text{O}}/\text{MGPC}$  value is nearly equivalent, and the measured  $\Delta m_{\text{EG}}/\text{MGPC}$  value is slightly lower compared with the predicted values.

The mass gains during the first and third TMA exposures are less than the mass gain of ~32 ng/cm<sup>2</sup> observed during TMA exposure for Al<sub>2</sub>O<sub>3</sub> ALD at 125 °C.<sup>37</sup> However, the mass gains of +12 and +10 ng/cm<sup>2</sup> are very similar to the mass gain of +10 ng/cm<sup>2</sup> observed during TMA exposure for alucone MLD using TMA and EG at 135 °C.<sup>12</sup> The smaller mass gains during the TMA exposure are explained by double reactions during the EG exposure that remove active –OH surface sites.<sup>12</sup> The slightly negative mass loss of -1 ng/cm<sup>2</sup> during the H<sub>2</sub>O exposure can be attributed to the replacement of –CH<sub>3</sub> species with –OH species and the concurrent desorption of a small amount of TMA from the previous TMA exposure.<sup>12</sup>

Figures 5a,b show the QCM results for the growth of 50 reactant sequences for the 1:1 alucone alloy and 25 reactant sequences for the 3:1 alucone alloy, respectively, at 135 °C. The alucone alloy growth was initiated on an Al<sub>2</sub>O<sub>3</sub> ALD substrate. The alucone alloy growth nucleated rapidly and quickly reached steady state growth conditions. After the short nucleation period, the mass gain was extremely linear versus the number of

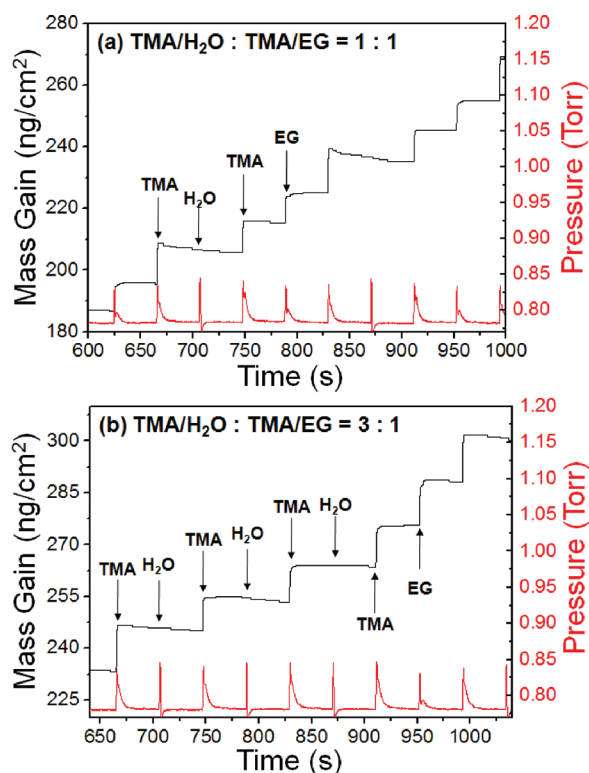


**Figure 4.** Mass gain and reactor pressure during the growth of alucone alloy films at 135 °C in the steady state regime: (a) 1:1 alucone alloy and (b) 3:1 alucone alloy.

steady state growth at 135°. The timing sequences for the ALD and MLD processes were (1, 40, 1, 40). The mass gain is stepwise with each reactant exposure. The alucone alloy films

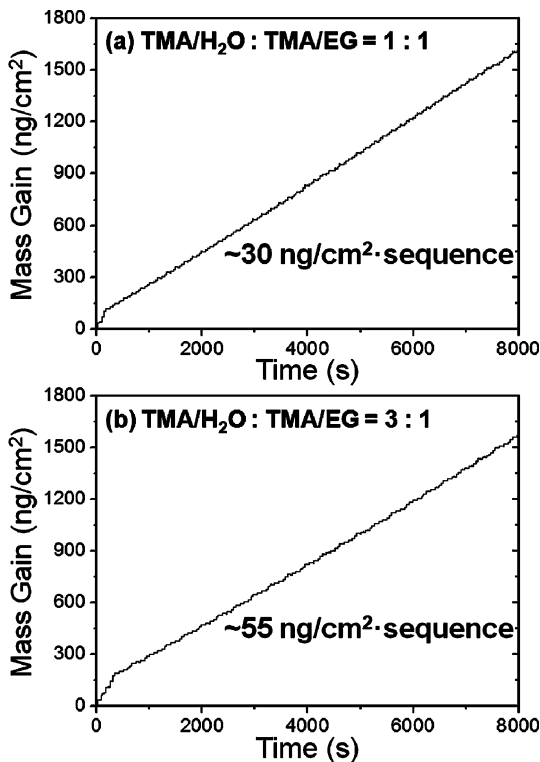


**Figure 5.** Mass gain versus number of reactant sequences at 135 °C for (a) 1:1 alucone alloy and (b) 3:1 alucone alloy.

reactant sequences. The 1:1 alucone alloy had a growth rate of  $\sim 30 \text{ ng/cm}^2$  sequence. The 3:1 alucone alloy had a growth rate of  $\sim 55 \text{ ng/cm}^2$  sequence.

The alucone alloy growth was also analyzed using *ex situ* XRR analysis. The alucone alloy films were grown on Si wafers with a native SiO<sub>2</sub> oxide. The film thickness was determined after various numbers of ALD/MLD cycles. The fitting of the XRR scan accounted for the alucone alloy film and the native SiO<sub>2</sub> oxide film on the Si wafer. The results for film thickness versus number of reactant sequences are shown in Figure 6. The growth rates are  $\sim 3.1$ ,  $\sim 5.7$ , and  $\sim 7.7 \text{ \AA}/\text{sequence}$  for the 1:1, 3:1, and 1:3 alucone alloys, respectively.

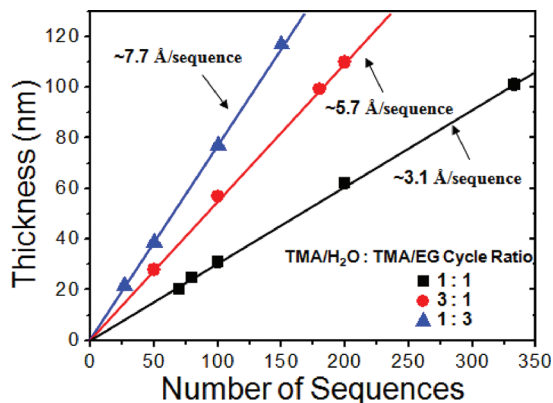


**Figure 6.** Film thickness measured using XRR versus number of reactant sequences for 1:1, 3:1, and 1:3 alucone alloy films.

The growth rate is higher for the alucone alloys that have a higher proportion of alucone MLD cycles. This behavior is approximately consistent with the growth rates of Al<sub>2</sub>O<sub>3</sub> ALD

and alucone MLD. At 135 °C, the Al<sub>2</sub>O<sub>3</sub> ALD growth rate is 1.1 Å/cycle and the alucone MLD growth rate is 1.5 Å/cycle.<sup>12,23–25</sup> The growth rates for the alucone alloys are not simply the sum of the individual Al<sub>2</sub>O<sub>3</sub> ALD and alucone MLD growth rates because of nucleation effects. The alucone alloy growth rates measured by *ex situ* XRR analysis and *in situ* QCM measurements also are in relative agreement. However, the thicknesses measured by XRR analysis are slightly larger than expectations based on the QCM mass measurements and the densities. These differences may be caused by changes in the alucone alloy films after ambient exposure.<sup>12</sup>

**3. Density, Stability, and Refractive Index.** The density of alucone alloy films grown on Si(100) substrates at 135 °C was also measured using *ex situ* XRR analysis. Figure 7 shows

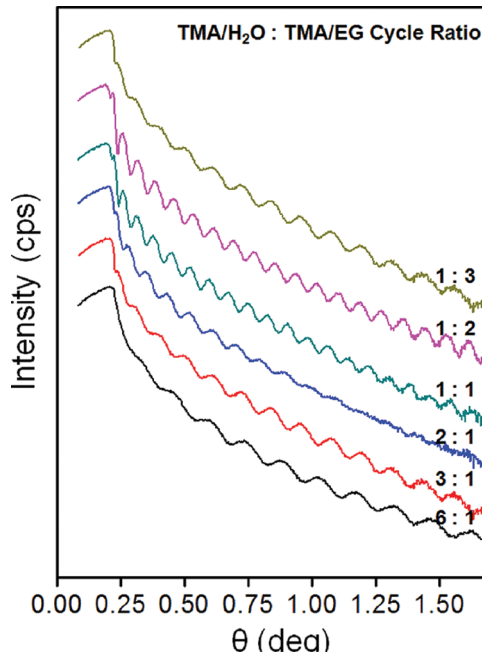


**Figure 7.** XRR scans of alucone alloy films with different TMA/H<sub>2</sub>O:TMA/EG cycle ratios.

XRR scans of the alucone alloy films grown with various ALD:MLD ratios. The scans display an oscillatory intensity as a function of the angle that drops over many orders of magnitude. This behavior is consistent with a very smooth and high quality film.

The critical angle,  $\Theta_c$ , of the XRR scans is related to the electron density,  $N_e$ , by  $N_e = (\Theta_c^2 \pi) / (\lambda^2 r_e)$ , where  $\lambda$  is the X-ray wavelength and  $r_e$  is the classical electron radius.<sup>38,39</sup> The mass density,  $\rho_m$ , can be related to the electron density by  $\rho_m = (N_e A) / (N_A Z)$ , where  $A$  is the average molar mass,  $Z$  is the average atomic number, and  $N_A$  is Avogadro's number.<sup>38,39</sup> A determination of  $\rho_m$  from the electron density requires knowledge of the film composition. Since the exact composition of the alucone alloys is not known, Figure 8 presents the electron density values derived from the XRR scans for alucone alloy films grown with different ALD:MLD ratios.

The electron densities vary from  $5.0 \times 10^{23} \text{ e}^-/\text{cm}^3$  for pure alucone MLD films to  $8.9 \times 10^{23} \text{ e}^-/\text{cm}^3$  for pure Al<sub>2</sub>O<sub>3</sub> ALD films. Assuming compositions of  $-\text{AlO}(\text{CH}_2)_2\text{O}-$  for alucone and Al<sub>2</sub>O<sub>3</sub> for Al<sub>2</sub>O<sub>3</sub>, the mass densities of the pure alucone film and Al<sub>2</sub>O<sub>3</sub> film are 1.6 and 3.0 g/cm<sup>3</sup>, respectively. These mass

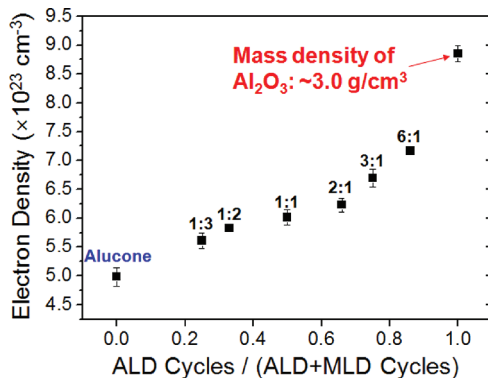


Figure 8. Electron density versus fraction of ALD cycles expressed as ALD cycles/(ALD + MLD cycles) for the alucone alloy films.

densities agree well with previous measurements of  $1.5 \text{ g/cm}^3$  for alucone MLD films and  $3.0 \text{ g/cm}^3$  for  $\text{Al}_2\text{O}_3$  ALD films.<sup>12</sup> For the alucone alloys, the density increases gradually and relatively smoothly with the increasing fraction of ALD cycles expressed as ALD cycles/(ALD + MLD cycles). This result indicates that the density of the alucone alloy films can be precisely tuned by varying the relative number of TMA/ $\text{H}_2\text{O}$  and TMA/EG cycles during the alucone alloy film growth.

To investigate the stability of the alucone alloys in air, films with different ALD:MLD ratios were deposited on silicon substrates. The film thickness was then measured using XRR analysis. The 1:1 alucone alloy film was grown using 200 reactant sequences. The 3:1 and 1:3 alucone alloy films were both grown using 100 reactant sequences. For comparison, 200 cycles of a pure alucone MLD film was also grown using only TMA and EG exposures. These XRR studies revealed that the pure alucone MLD film thickness decreased  $\sim 23\%$  during the first week. This decrease is consistent with previous studies of alucone MLD film stability.<sup>12</sup> The 1:3 alucone alloy film thickness also decreased  $\sim 6\%$  after 1 week. In contrast, no thickness change was observed for the 1:1 and 3:1 alucone alloy films after 1 week. These observations indicate that the alucone alloy films with a higher proportion of TMA/ $\text{H}_2\text{O}$  cycles are stable. The  $\text{Al}_2\text{O}_3$  fraction in the alucone alloys helps prevent any chemical change that can lead to film shrinkage.<sup>12</sup>

The refractive indices obtained from the spectroscopic ellipsometry measurements are shown in Figure 9. The refractive indices varied from  $n = 1.45$  for pure alucone MLD films to  $n = 1.64$  for pure  $\text{Al}_2\text{O}_3$  ALD films. The refractive index

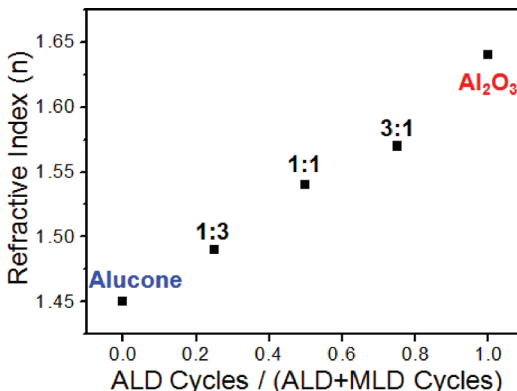


Figure 9. Refractive index measured using ellipsometry versus fraction of ALD cycles for the alucone alloy films.

changes progressively with the increasing fraction of ALD cycles during film growth. This change is expected based on the relationship between density and refractive index given by the Lorenz–Lorentz equation.<sup>40</sup>

**4. Elastic Modulus and Hardness.** Nanoindentation measurements were utilized to measure the elastic modulus and hardness of the alucone alloy films. Figure 10 displays the load versus displacement curves for the pure alucone MLD film, various alucone alloy films, and the pure  $\text{Al}_2\text{O}_3$  ALD film.

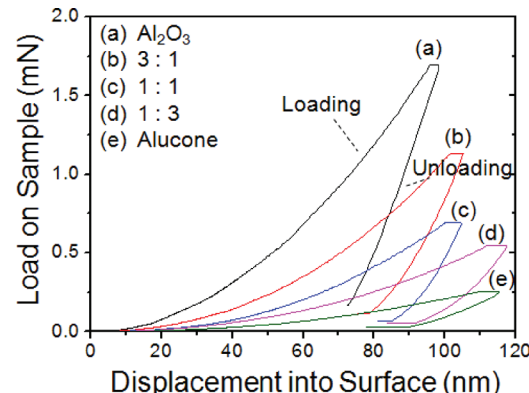


Figure 10. Load vs displacement curves from nanoindentation measurements for pure  $\text{Al}_2\text{O}_3$ , pure alucone, and alucone alloy films with cycle ratios of 3:1, 1:1, and 1:3.

These measurements were consistent 1 day, 1 week, 2 weeks, and 1 month after growing the alucone alloy films. The elastic modulus and hardness were derived from the load versus displacement curves.

The elastic modulus,  $E$ , is displayed in Figure 11a. In agreement with previous measurements,<sup>27,41</sup> the elastic modulus of the pure alucone MLD film and pure  $\text{Al}_2\text{O}_3$  ALD film are  $E = 21 \pm 8 \text{ GPa}$  and  $E = 198 \pm 8 \text{ GPa}$ , respectively. The elastic modulus progressively increases for the 1:3, 1:1, and 3:1 alucone alloys before increasing more dramatically to  $E = 198 \pm 8 \text{ GPa}$  for the pure  $\text{Al}_2\text{O}_3$  ALD film. The magnitude for the elastic modulus is higher for larger  $\text{Al}_2\text{O}_3$  fractions in the alucone alloy films.

The elastic modulus values can be compared with predictions based on rule-of-mixtures approximations.<sup>42</sup> The upper bound for the rule-of-mixtures approximation can be expressed as

$$E_U = E_1 M_1 + E_2 M_2 \quad (1)$$

The lower bound for the rule-of-mixtures approximation is given by

$$E_L = E_1 E_2 / (E_1 M_2 + E_2 M_1) \quad (2)$$

In these equations,  $E_1$  and  $E_2$  are the elastic moduli for the  $\text{Al}_2\text{O}_3$  ALD and alucone MLD films, respectively.  $M_1$  and  $M_2$  are the mass gain fractions for the  $\text{Al}_2\text{O}_3$  ALD and alucone MLD components, respectively, of the total mass gain for the reaction sequence. The mass gain fractions are estimates for the volume fractions. Figure 11a shows that the measured elastic moduli are contained within the upper and lower bounds.

The hardness,  $H$ , is shown in Figure 11b. The hardness of the pure alucone MLD film and pure  $\text{Al}_2\text{O}_3$  ALD film are  $H = 1.0 \pm 0.1 \text{ GPa}$  and  $H = 13.0 \pm 0.2 \text{ GPa}$ , respectively. These values agree with previous measurements.<sup>27,43</sup> Compared with the pure alucone MLD film, the hardness progressively increases for the 1:3, 1:1, and 3:1 alucone alloys. The hardness

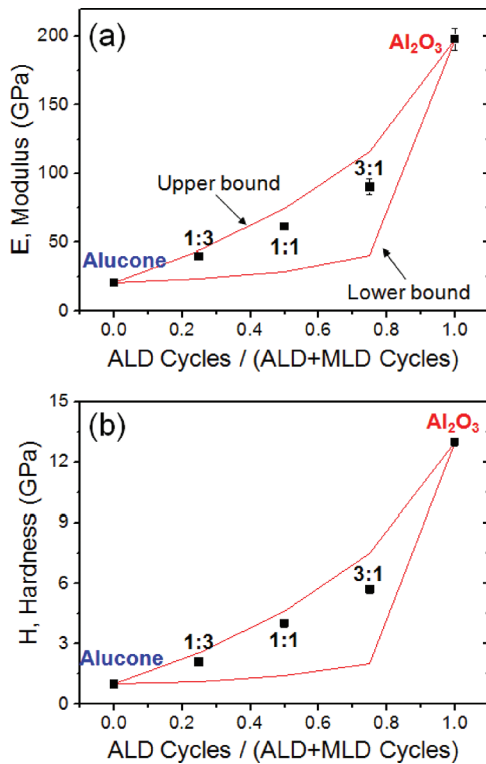


**Figure 11.** Elastic modulus and hardness versus fraction of ALD cycles for the alucone alloy films.

then increases more dramatically to  $H = 13.0 \pm 0.2$  GPa for the pure  $\text{Al}_2\text{O}_3$  ALD film. In similarity to the elastic modulus, the magnitude for the hardness is higher for larger  $\text{Al}_2\text{O}_3$  fractions in the alucone alloy films.

Predictions for the hardness can also be obtained from the rule-of-mixtures approximations.<sup>42</sup> Upper and lower bounds for the hardness are similar to the upper and lower bounds for the elastic modulus given in eqs 1 and 2. Mass gain fractions are again employed to estimate the volume fractions. Figure 11b shows that the measured hardness values are contained within the predicted upper and lower bounds.

##### 5. Multilayer of Alucone Alloy with $\text{Al}_2\text{O}_3$ ALD Layers.

Multilayers of alucone alloys and  $\text{Al}_2\text{O}_3$  ALD layers may be useful for flexible multilayer coatings.<sup>44,45</sup> These flexible multilayers may be valuable as flexible gas diffusion barriers.<sup>46</sup> The flexible alucone alloy may decouple the more brittle  $\text{Al}_2\text{O}_3$  ALD layers and allow the composite multilayer to achieve a higher critical tensile strain than the individual  $\text{Al}_2\text{O}_3$  ALD layers.<sup>44</sup> Figure 12 displays a cross-sectional transmission electron microscopy (TEM) image of an  $\text{Al}_2\text{O}_3$  ALD/1:1 alucone alloy/ $\text{Al}_2\text{O}_3$  ALD trilayer deposited on a Si(100) substrate at 135 °C.

The contrast between the  $\text{Al}_2\text{O}_3$  ALD layers and the 1:1 alucone alloy layer is caused by the lower density of the 1:1 alucone alloy layer. The interfaces between the  $\text{Al}_2\text{O}_3$  ALD layer and the 1:1 alucone alloy layer are very smooth. The 1:1 alucone alloy film is deposited very conformally on the  $\text{Al}_2\text{O}_3$  ALD layer. The thickness of the 1:1 alucone alloy film is ~6.1 nm. The 1:1 alucone alloy film was deposited using 20 TMA/H<sub>2</sub>O/TMA/EG sequences. The measured thickness is in agreement with the growth rate of ~3.1 Å/sequence for the 1:1 alucone alloy determined by the XRR measurements in Figure 6.

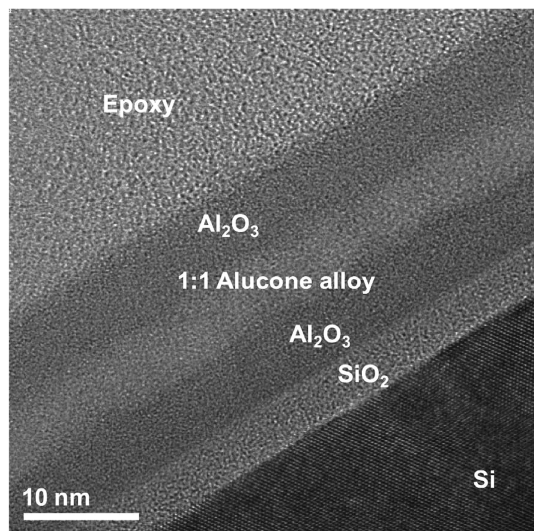


**Figure 12.** TEM image of 1:1 alucone alloy film sandwiched between two  $\text{Al}_2\text{O}_3$  ALD films.

## IV. CONCLUSIONS

Alucone alloy films were fabricated by combining  $\text{Al}_2\text{O}_3$  ALD and alucone MLD at 135 °C. The composition of alucone alloy films was controlled by adjusting the relative number of TMA/H<sub>2</sub>O cycles for  $\text{Al}_2\text{O}_3$  ALD and TMA/EG cycles for alucone MLD in the reactant pulse sequence. Alucone alloys were grown using a relative number of  $\text{Al}_2\text{O}_3$  ALD and alucone MLD cycles varying from 1:3 to 6:1 (TMA/H<sub>2</sub>O: TMA/EG). Linear growth and self-limiting surface reactions were observed for all the alucone alloys. These alucone alloys also displayed varying density, refractive index, elastic modulus, and hardness as the composition changed from the pure alucone MLD film to the pure  $\text{Al}_2\text{O}_3$  ALD film. The density and refractive index varied from 1.6 g/cm<sup>3</sup> and  $n = 1.45$  for pure alucone to 3.0 g/cm<sup>3</sup> and  $n = 1.64$  for pure  $\text{Al}_2\text{O}_3$ , respectively. The elastic modulus and hardness changed from  $21 \pm 8$  GPa and  $1.0 \pm 0.1$  GPa for pure alucone to  $198 \pm 8$  GPa and  $13.0 \pm 0.2$  GPa for pure  $\text{Al}_2\text{O}_3$ , respectively. These results demonstrate the capability of ALD/MLD alloy films to provide tunable properties. These alucone alloys should be useful for many functional film applications.

## ACKNOWLEDGMENTS

This research was funded by DuPont Central Research and Development, the National Science Foundation (CHE-1012116), and the Air Force Office of Scientific Research (AFOSR). We thank Prof. Myung M. Sung at Hanyang University for obtaining the TEM images of the  $\text{Al}_2\text{O}_3$  ALD/alucone alloy multilayers. We also thank Noemi Leick for discussions regarding spectroscopic ellipsometry and the refractive index of the alucone alloy films.

## REFERENCES

- Suntola, T. *Thin Solid Films* **1992**, *216*, 84.
- Kim, H.; Lee, H.-B.-R.; Maeng, W.-J. *Thin Solid Films* **2009**, *517*, 2563.
- George, S. M.; Ott, A. W.; Klaus, J. W. *J. Phys. Chem.* **1996**, *100*, 13121.
- George, S. M. *Chem. Rev.* **2010**, *110*, 111.
- Leskela, M.; Ritala, M. *Thin Solid Films* **2002**, *409*, 138.
- Ritala, M.; Leskela, M. In *Handbook of Thin Film Materials*; Nalwa, H. S., Ed.; Academic Press: San Diego, CA, 2001; Vol. 1.

- (7) George, S. M.; Yoon, B.; Dameron, A. A. *Acc. Chem. Res.* **2009**, *42*, 498.
- (8) Shao, H.-I.; Umemoto, S.; Kikutani, T.; Okui, N. *Polymer* **1997**, *38*, 459.
- (9) Adamczyk, N. M.; Dameron, A. A.; George, S. M. *Langmuir* **2008**, *24*, 2081.
- (10) Putkonen, M.; Harjuoja, J.; Sajavaara, T.; Niinisto, L. *J. Mater. Chem.* **2007**, *17*, 664.
- (11) Yoshimura, T.; Tatsuura, S.; Sotoyama, W.; Matsuura, A.; Hayano, T. *Appl. Phys. Lett.* **1992**, *60*, 268.
- (12) Dameron, A. A.; Seghete, D.; Burton, B. B.; Davidson, S. D.; Cavanagh, A. S.; Bertrand, J. A.; George, S. M. *Chem. Mater.* **2008**, *20*, 3315.
- (13) Klepper, K. B.; Nilsen, O.; Fjellvag, H. *Dalton Trans.* **2010**, *39*, 11628.
- (14) Klepper, K. B.; Nilsen, O.; Hansen, P. A.; Fjellvag, H. *Dalton Trans.* **2011**, *40*, 4636.
- (15) Lee, B. H.; Lee, K. H.; Im, S.; Sung, M. M. *Org. Electron.* **2008**, *9*, 1146.
- (16) Lee, B. H.; Ryu, M. K.; Choi, S. Y.; Lee, K. H.; Im, S.; Sung, M. *M. J. Am. Chem. Soc.* **2007**, *129*, 16034.
- (17) Seghete, D.; Hall, R. A.; Yoon, B.; George, S. M. *Langmuir* **2010**, *26*, 19045.
- (18) Yoon, B.; Patchen, J. L. O.; Seghete, D.; Cavanagh, A. S.; George, S. M. *Chem. Vap. Deposition* **2009**, *15*, 112.
- (19) Yoon, B.; Seghete, D.; Cavanagh, A. S.; George, S. M. *Chem. Mater.* **2009**, *21*, 5365.
- (20) George, S. M.; Lee, B. H.; Yoon, B.; Abdulagatov, A. I.; Hall, R. *A. J. Nanosci. Nanotechnol.* **2011**, *11*, 7948.
- (21) Peng, Q.; Gong, B.; VanGundy, R. M.; Parsons, G. N. *Chem. Mater.* **2009**, *21*, 820.
- (22) Dillon, A. C.; Ott, A. W.; Way, J. D.; George, S. M. *Surf. Sci.* **1995**, *322*, 230.
- (23) Groner, M. D.; Fabreguette, F. H.; Elam, J. W.; George, S. M. *Chem. Mater.* **2004**, *16*, 639.
- (24) Ott, A. W.; Klaus, J. W.; Johnson, J. M.; George, S. M. *Thin Solid Films* **1997**, *292*, 135.
- (25) Elam, J. W.; Groner, M. D.; George, S. M. *Rev. Sci. Instrum.* **2002**, *73*, 2981.
- (26) Ferguson, J. D.; Weimer, A. W.; George, S. M. *Thin Solid Films* **2000**, *371*, 95.
- (27) Miller, D. C.; Foster, R. R.; Jen, S.; Bertrand, J. A.; Seghete, D.; Yoon, B.; Lee, Y.; George, S. M.; Dunn, M. L. *Acta Mater.* **2009**, *57*, 5083.
- (28) Oliver, W. C.; Pharr, G. M. *J. Mater. Res.* **2004**, *19*, 3.
- (29) Joslin, D. L.; Oliver, W. C. *J. Mater. Res.* **1990**, *5*, 123.
- (30) Bobji, M. S.; Biswas, S. K.; Pethica, J. B. *Appl. Phys. Lett.* **1997**, *71*, 1059.
- (31) Tadjiev, D. R.; Hand, R. J.; Hayes, S. A. *Philos. Mag.* **2010**, *90*, 1819.
- (32) Jian, S. R.; Jang, J. S. C.; Chen, G. J.; Chen, H. G.; Chen, Y. T. *J. J. Alloys Compd.* **2009**, *479*, 348.
- (33) Saha, R.; Nix, W. D. *Acta Mater.* **2002**, *50*, 23.
- (34) Dillon, A. C.; Ott, A. W.; Way, J. D.; George, S. M. *Surf. Sci.* **1995**, *322*, 230.
- (35) Ferguson, J. D.; Yoder, A. R.; Weimer, A. W.; George, S. M. *Appl. Surf. Sci.* **2004**, *226*, 393.
- (36) Ferguson, J. D.; Weimer, A. W.; George, S. M. *J. Vac. Sci. Technol., A* **2005**, *23*, 118.
- (37) Wind, R. A.; George, S. M. *J. Phys. Chem. A* **2010**, *114*, 1281.
- (38) Holy, V.; Pietsch, U.; Baumbach, T. *High Resolution X-ray Scattering from Thin Films and Multilayers*; Springer-Verlag: Berlin, 1999.
- (39) Phung, T. M.; Jensen, J. M.; Johnson, D. C.; Donovan, J. J.; McBurnett, B. G. *X-Ray Spectrom.* **2008**, *37*, 608.
- (40) Huang, Y. Y.; Sarkar, A.; Schultz, P. C. *J. Non-Cryst. Solids* **1977**, *27*, 29.
- (41) Tapily, K.; Jakes, J. E.; Stone, D. S.; Shrestha, P.; Gu, D.; Baumgart, H.; Elmustafa, A. A. *J. Electrochem. Soc.* **2008**, *155*, H545.
- (42) Callister, W. D., Jr.; Rethwisch, D. G. *Materials Science and Engineering: An Introduction*, 8th ed.; John Wiley & Sons, Inc.: Hoboken, NJ, 2010.
- (43) Tripp, M. K.; Stampfer, C.; Miller, D. C.; Helbling, T.; Herrmann, C. F.; Hierold, C.; Gall, K.; George, S. M.; Bright, V. M. *Sens. Actuators, A* **2006**, *130–131*, 419.
- (44) Cordero, N.; Yoon, J.; Suo, Z. G. *Appl. Phys. Lett.* **2007**, *90*.
- (45) Miller, D. C.; Foster, R. R.; Zhang, Y. D.; Jen, S. H.; Bertrand, J. A.; Lu, Z. X.; Seghete, D.; O'Patchen, J. L.; Yang, R. G.; Lee, Y. C.; George, S. M.; Dunn, M. L. *J. Appl. Phys.* **2009**, *105*.
- (46) Graff, G. L.; Williford, R. E.; Burrows, P. E. *J. Appl. Phys.* **2004**, *96*, 1840.